International Journal of Minerals, Metallurgy and Materials
Volume 24, Number 9, September 2017, Page 1043
DOI: 10.1007/s12613-017-1494-2

Structural, morphological, and optical properties of tin(IV) oxide nanoparticles synthesized using *Camellia sinensis* extract: a green approach

J. Celina Selvakumari, M. Ahila, M. Malligavathy, and D. Pathinettam Padiyan

Department of Physics, Manonmaniam Sundaranar University, Tirunelveli 627012, Tamil Nadu, India
(Received: 28 November 2016; revised: 26 April 2017; accepted: 28 April 2017)

Abstract: Tin oxide (SnO_2) nanoparticles were cost-effectively synthesized using nontoxic chemicals and green tea (*Camellia sinensis*) extract via a green synthesis method. The structural properties of the obtained nanoparticles were studied using X-ray diffraction, which indicated that the crystallite size was less than 20 nm. The particle size and morphology of the nanoparticles were analyzed using scanning electron microscopy and transmission electron microscopy. The morphological analysis revealed agglomerated spherical nanoparticles with sizes varying from 5 to 30 nm. The optical properties of the nanoparticles' band gap were characterized using diffuse reflectance spectroscopy. The band gap was found to decrease with increasing annealing temperature. The O vacancy defects were analyzed using photoluminescence spectroscopy. The increase in the crystallite size, decreasing band gap, and the increasing intensities of the UV and visible emission peaks indicated that the green-synthesized SnO_2 may play future important roles in catalysis and optoelectronic devices.

Keywords: tin oxide; nanoparticles; *Camellia sinensis*; band gap; photoluminescence

1. Introduction

Tin(IV) oxide (SnO_2) nanoparticles have a large variety of applications in the fields of catalysis [1], energy storage [2], sensors [3], dye-sensitized solar cells [4], medicine [5], and optoelectronics [6] because of their unique physical and chemical properties [7]. Compared with the bulk material, the transformed nanostructures have received greater attention in recent research because of their improved properties [8]. SnO_2 is an n-type semiconductor with a direct band-gap energy of ~3.6 eV [9]. Because of its large band-gap, it exhibits remarkable sensitivity in gas sensor applications [10]. Because of its high specific area, good stability, and low density, it is used in sensors to improve their response time and sensitivity [11]. Its large number of active sites, high surface response, and strong radiation absorption enhance the photocatalytic removal of dyes [12]. It is used as an anode material in Li-ion batteries with high theoretical capacity [13]. In addition, the band-gap of SnO_2 nanoparticles responds to UV irradiation, making it useful in solar cells [14].

SnO_2 nanoparticles with various shapes and sizes have been synthesized using sol–gel [15], precipitation [16], hydrothermal [17], solvothermal [18], and green synthesis methods [19]. Among these methods, the green synthesis of nanoparticles using leaf extracts is an eco-friendly process involving nontoxic reagents. Haritha *et al*. [20] prepared SnO_2 nanoparticles with a crystallite size of 47 nm using the root bark extract of *Catunaregam spinosa*. Fu *et al*. [21] achieved 91% of photodegradation of rhodamine B dye in the presence of SnO_2 nanoparticles prepared using *Plectranthus amboinicus* leaf extract. Bhattacharjee *et al*. [22] used urea in the synthesis of SnO_2 nanoparticles via a green method involving microwave heating and obtained 4-nm quantum dots that degrade eosin Y dye more effectively than commercially obtained SnO_2. Zheng *et al*. [23] used *Corymbia citriodora* leaf extract to synthesize polyhedron-shaped ZnO nanoparticles and investigated their photocatalytic performance toward the degradation of methylene blue.

Nishant and Mausumi [24] used Gram-negative bacterium *Erwinia herbicola* to prepare 15–40 nm SnO_2 nanoparticles to degrade organic dyes. Zheng *et al*. [25] prepared

Corresponding author: D. Pathinettam Padiyan E-mail: dppadiyan@msuniv.ac.in

reduced graphene oxide (RGO)–Ag nanocomposites with a crystallite size of 18.7 nm using *Plectranthus amboinicus* leaf extract. Begum *et al*. [26] also studied dye removal using 5-nm SnO_2 nanoparticles prepared using L-lysine monohydrate as a mediator. Diallo *et al*. [19] synthesized SnO_2 nanoparticles with diameters less than 20 nm using *Aspalathus linearis* and observed that the smallest SnO_2 nanoparticles exhibited effective photocatalytic properties. Elango and Roopan [27] prepared 21-nm SnO_2 nanoparticles using *Cyphomandra betacea* extract and characterized their photocatalytic degradation of methylene blue. Fu and Fu [28] synthesized photocatalytically active ZnO nanoparticles with emission in the UV region using *Plectranthus amboinicus* leaf extract.

Thus, on the basis of the aforementioned studies, the controlled size and morphology of nanoparticles clearly plays an important role in various photocatalytic applications. To the best of our knowledge, the synthesis of SnO_2 nanoparticles using green tea extract has not yet been reported. The purpose of this work is to study the structural and optical properties of SnO_2 nanoparticles synthesized using green tea (*Camellia sinensis*) extract. The polyphenolic compounds present in green tea, which are called catechins, undergo oxidation [29]. These compounds exhibit antioxidant properties and function as reducing agents of metal ions during the green synthesis of SnO_2 nanoparticles.

2. Experimental

2.1. Materials

Purified tin(II) chloride ($SnCl_2$) was purchased from Merck. The leaves of green tea were purchased from Supriya Tea Co., Kerala, India. Deionized water was used throughout the experiments.

2.2. Method

2.2.1. Extract preparation

A weighed 5-g sample of green tea leaves was added to 100 mL of double-distilled water; the resulting mixture was heated at 80°C for 20 min and then filtered. The filtered extract was stored in a refrigerator until further use.

2.2.2. Synthesis of SnO_2 nanoparticles

50 mL of 0.05 M $SnCl_2$ solution was added to 50 mL of the aforementioned extract, and the resulting mixture was heated at 80°C for 30 min. The formed precipitates were centrifuged to remove the residual particles and then dried in an oven at 80°C. This as-prepared sample was labeled as T0. The precipitates were then annealed at 200, 400, 600, and 800°C, and the obtained samples were labeled T2, T4, T6, and T8, respectively.

2.2.3. Mechanism

The polyphenols found in green tea act as an antioxidant. They include four flavanol derivatives: epicatechin (EC), epigallocatechin (EGC), epicatechin gallate (ECG), and epigallocatechin gallate (EGCG). These polyphenols can function as both reducing and stabilizing agents [30]. The formation of SnO_2 nanoparticles occurs through (i) reduction of Sn^{2+} to Sn^0, (ii) the reducing effect of phenolic compounds (–OH) of green tea extract to form Sn species, and (iii) a phase transformation of the Sn species into SnO_2 nanoparticles at higher annealing temperatures. The reduction of Sn^{2+} occurs via the –OH groups in EGCG which serve as both stabilizing and capping agents during the reaction [31]. EGCG is strongly polar and highly water soluble; it acts as a stable (electron + proton) donor in interactions, and can be converted into a radical ion ("semihydro-EGCG") and then into dehydro-EGCG through oxidation. The redox reaction of Sn^{2+} to Sn^0 occurs through a combination of dehydro-EGCG and EGCG(–OH) groups. The lone pairs of electrons in the polar groups of EGCG occupy 2 sp orbitals of an Sn^{2+} ion to form an Sn^{2+} complex. The reduction of Sn^{2+} capped with the phenolic compounds forms Sn^0 nanoparticles inside the nanoscopic templates. In this nanoscale template, small Sn^0 nanoparticles are easily formed. Upon air annealing, SnO_2 nanoparticles are formed via oxidation of Sn^0 [30,32]. The mechanism for the synthesis of SnO_2 is shown in Fig. 1.

2.3. Characterization

The crystal structure and crystallite sizes were determined from the X-ray diffraction (XRD) patterns recorded using a PANalytical Xpert-Pro X-ray diffractometer equipped with a Cu K_α radiation source; the samples were scanned over the 2θ range from 10° to 80°. The microstructure morphology of the nanoparticles was investigated by high-resolution transmission electron microscopy (HR-TEM) on a JEOL JEM 2100. The optical reflectance was characterized using UV–Vis diffuse reflectance spectroscopy (DRS; Shimadzu UV-2700) in the wavelength range from 220 to 800 nm; $BaSO_4$ was used as a standard. The surface morphology was analyzed using high-resolution scanning electron microscopy (HR-SEM) carried out on an FEI Quanta FEG 200. The nanoparticles' elemental composition was obtained by energy-dispersive X-ray (EDX) analysis conducted using a spectrometer attached to the scanning electron microscope. A Cary Eclipse EL08083851 fluorescence spectrophotometer was used to collect the photoluminescence (PL) spectra with an excitation wavelength of 310 nm.

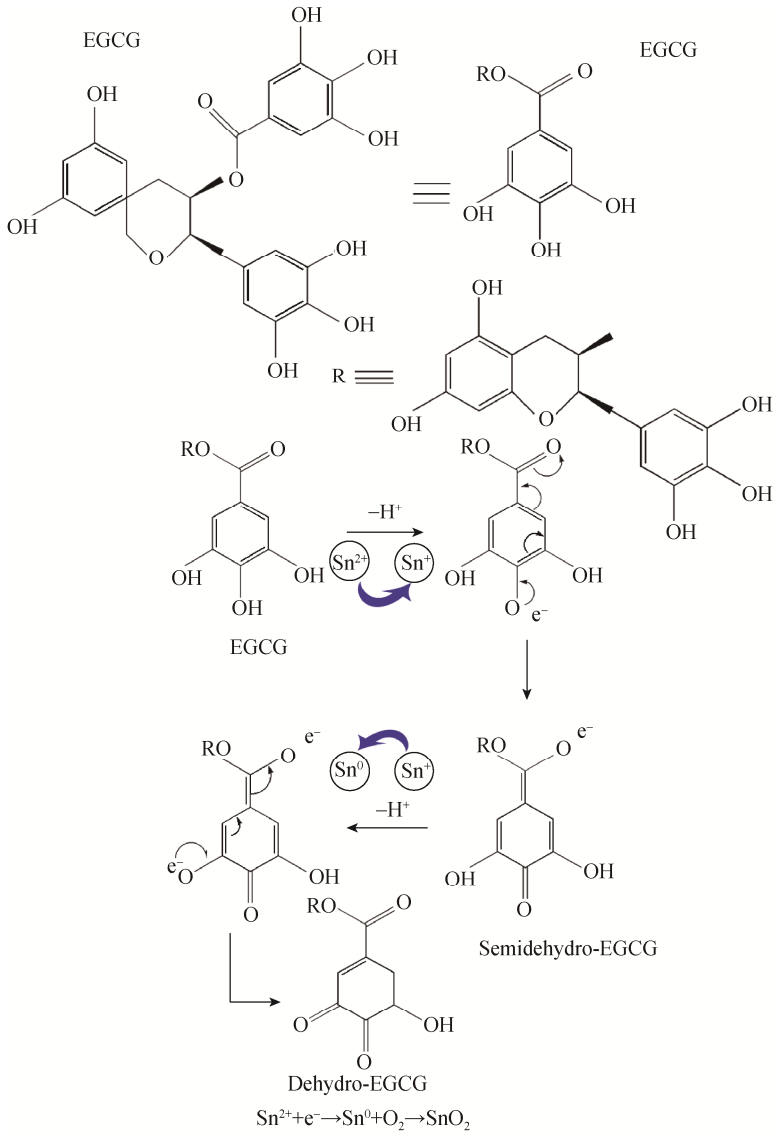

Fig. 1. Reaction mechanism for the formation of SnO_2 nanoparticles.

3. Results and discussion

3.1. X-ray diffraction analysis

The XRD patterns of the green-synthesized SnO_2 nanoparticles (T0, T2, T4, T6, and T8) are shown in Fig. 2. The patterns of the T0 and T2 samples do not show any XRD peaks, indicating that these samples are amorphous. In the case of the sample annealed at 400°C, the crystallinity improved, resulting in the appearance of diffraction peaks at 26.89°, 33.45°, 51.34°, and 65.2°, which are ascribed to the (110), (101), (211), and (301) planes, respectively. In the case of sample T6, seven diffraction peaks appear at 2θ angles of 26.59°, 34.22°, 38.05°, 51.97°, 62.06°, 65.96°, and 71.38°; these peaks are related to the (110), (101), (200), (211), (310), (301), and (202) lattice planes, respectively. The obtained 2θ values for sample T8 are 26.81°, 34.07°, 37.38°, 52.01°, 54.88°, 62.07°, 66.15°, and 71.47°, which are associated with the (110), (101), (200), (211), (220), (310), (301), and (202) planes, respectively. The observed peaks of SnO_2 match well with the tetragonal structure given in JCPDS reference pattern No. (71-0652) [33]. Thus, the formation of tetragonal-structured SnO_2 nanoparticles is confirmed.

Diffraction peaks corresponding to Sn^0 were not present. The enhancement in the intensities of the diffraction peaks and the narrowing peak width with increasing annealing temperature clearly indicate the increases in crystallinity and crystallite size of the green-synthesized SnO_2 nanoparticles. Increased crystallinity in the order of T2 < T4 < T6 < T8 is clearly observed in the XRD patterns. Broad diffraction

peaks in XRD patterns indicate small particles. The crystallite size calculated on the basis of the full-width at half-maximum of the (110) plane using Scherrer's formula is 6.1, 8.1, and 16.1 nm for samples T4, T6, and T8, respectively. Nanoparticles with sizes less than 20 nm have distinct physical and chemical properties. The results presented here indicate that size-controlled SnO_2 can be synthesized by a green approach coupled with annealing.

3.2. HR-TEM analysis

Fig. 3 shows a microscopic view of SnO_2 nanoparticles; the first row clearly shows the morphology and particle size of the nanoparticles. Sample T2 exhibits no particular particle shape, possibly because of its amorphous nature. Upon annealing, the particles increase in size; spherical shapes are visible in T4. With a further increase in annealing temperature, spherical particles become distorted. Thus, an increase in annealing temperature results in larger particles [34] but with the odd shapes. The particle size varies in the range from 5 to 10 nm in the SnO_2 nanoparticle sample annealed at 600°C, as marked in the HR-TEM image of T6 (Fig. 3). In the case of the particles annealed at 800°C, the spherical shape observed in the case of T4 gives way to a hexagonal shape, as evident in the HR-TEM image of T8 (Fig. 3), which shows particles ranging in size from 16 to 31 nm. The average particle sizes of 8 and 20 nm were measured for samples T6 and T8, and these sizes agree well with the crystallite sizes calculated from the corresponding XRD patterns.

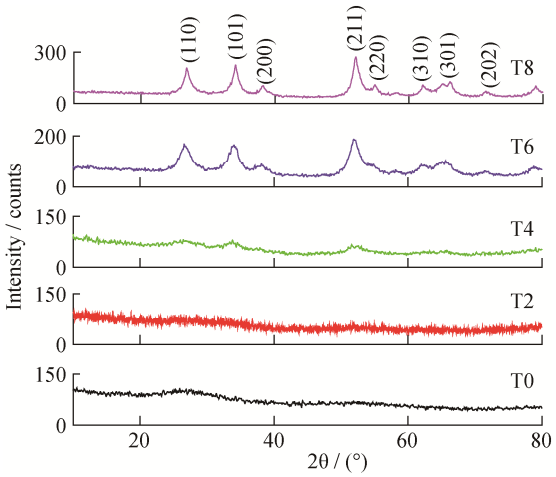

Fig. 2. XRD patterns of SnO_2 nanoparticles annealed at different temperatures.

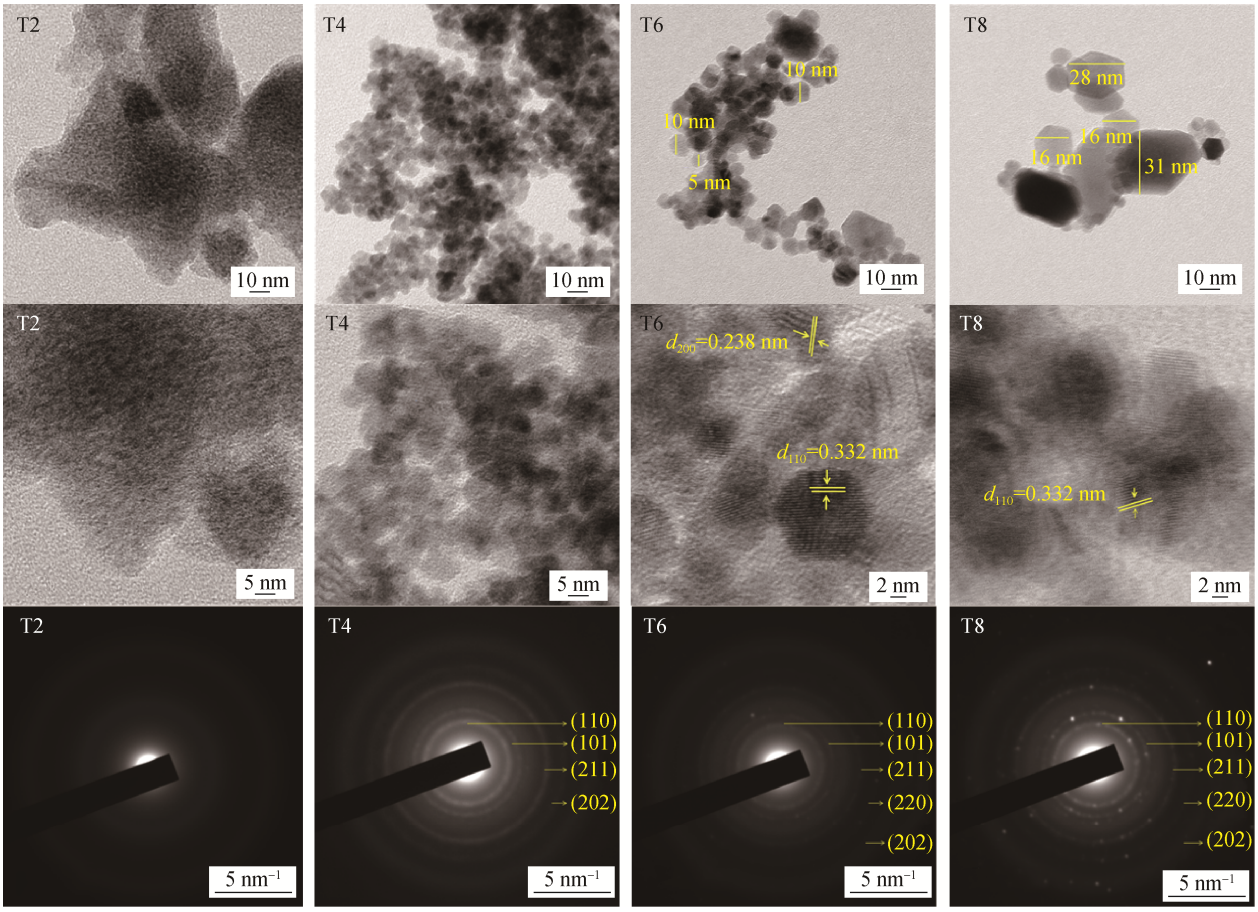

Fig. 3. TEM images of SnO_2 nanoparticles showing particle sizes (row 1), *d*-spacings (row 2), and SAED patterns (row 3).

The HR-TEM images of SnO_2 nanoparticles recorded at increased magnification are shown in the second row of Fig. 3. Lattice fringes are clearly observed in the images of T6 and T8 and are marked on the TEM images. The adjacent lattice spacing was found to be 0.332 nm in T6 and T8, which corresponds to the (110) plane of SnO_2. The vertical arrangement observed in the image of T6 (Fig. 3, second row) is related to the (200) plane with a lattice spacing of 0.238 nm, in good agreement with the XRD results.

The third row of Fig. 3 shows the selected area electron diffraction (SAED) patterns of SnO_2 nanoparticles. The weak diffused rings in the pattern of T2 are consistent with this sample's amorphous nature. With increasing annealing temperature, the crystallinity increases. The multiple rings observed in the TEM images denote the polycrystalline nature of SnO_2 nanoparticles, and the lattice plane (*hkl*) values of the rings confirm the tetragonal crystal structure of SnO_2.

3.3. HR-SEM analysis

The HR-SEM images reveal the macro morphology of the particles, as shown in Fig. 4. The particles are agglomerated with spherical-like morphology. The 2-nm hexagonal shapes observed in the TEM images in Fig. 3 are not clearly visible in the HR-SEM images at 500-nm magnification. The SEM images show numerous particles combined into a nearly spherical shape with nanoscale diameters. The particle size increases with increasing annealing temperature, in agreement with the XRD results.

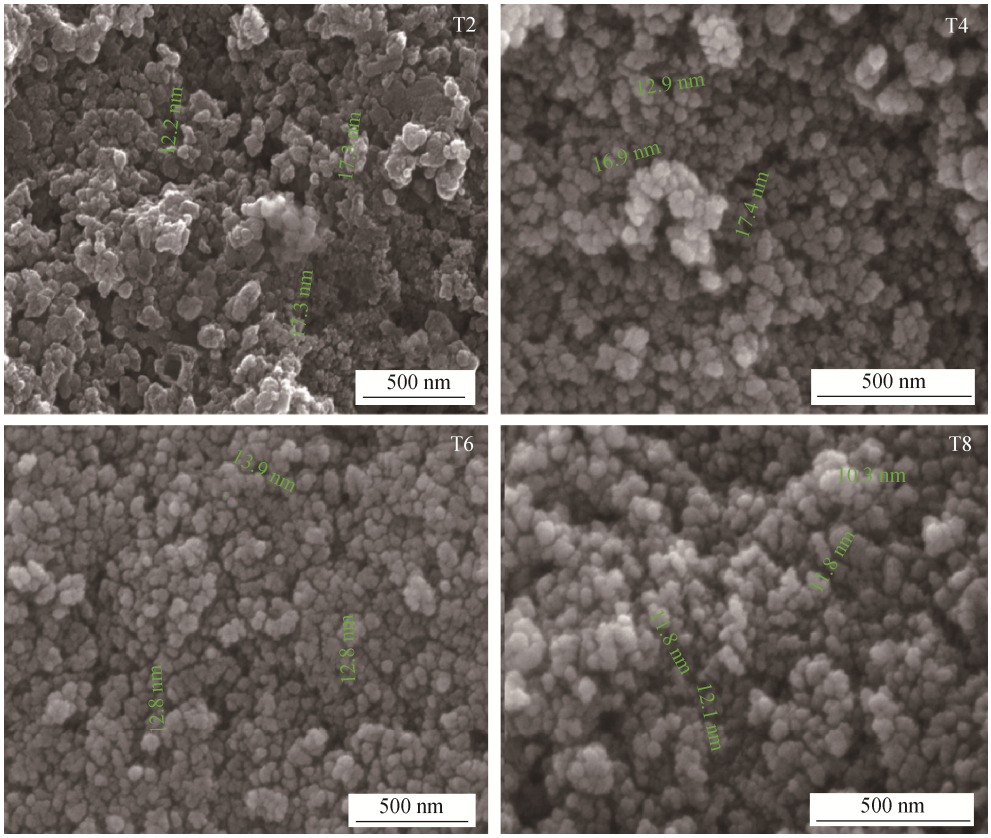

Fig. 4. SEM images of SnO_2 nanoparticles annealed at different temperatures.

The corresponding EDX patterns are shown in Fig. 5. In the sample annealed at 200°C, carbon is present as an impurity in addition to Sn and O. The peak at 2 keV is due to the Au coating on the samples prepared for SEM. The carbon impurities disappear with increasing annealing temperature, and the calculated weight percentages of 66.10% O and 33.90% Sn confirm the presence of Sn and O, as clearly evident in the EDX patterns.

3.4. Diffuse reflectance spectroscopy

DRS was used to determine the band-gap of the green-synthesized nanoparticles. The band-gap was analyzed using the Kulbelka–Munk equation:

$$K / S = (1 - R_\infty)^2 / 2R_\infty = F(R_\infty) = \alpha \quad (1)$$

where S is the scattering coefficient, K is the absorption coefficient, $R = R_{sample}/R_{standard}$, R_∞ is the reflectance of an

infinitely thick layer of the sample to hide the substrate and $F(R_\infty)$ is the Kubelka-Munk function.

The band-gap energy was obtained from the absorption spectra using the following equation:

$$F(R_\infty)h\upsilon = K(h\upsilon - E_g)^n \quad (2)$$

where hv is the incident photon energy, and E_g is the band-gap energy of the material. The exponent n denotes the transition type, where n = 1/2, 2, 3/2, and 3 for allowed direct, allowed indirect, forbidden direct, and forbidden indirect transitions, respectively. Here, n = 1/2, which indicates an allowed direct transition in SnO_2 nanoparticles.

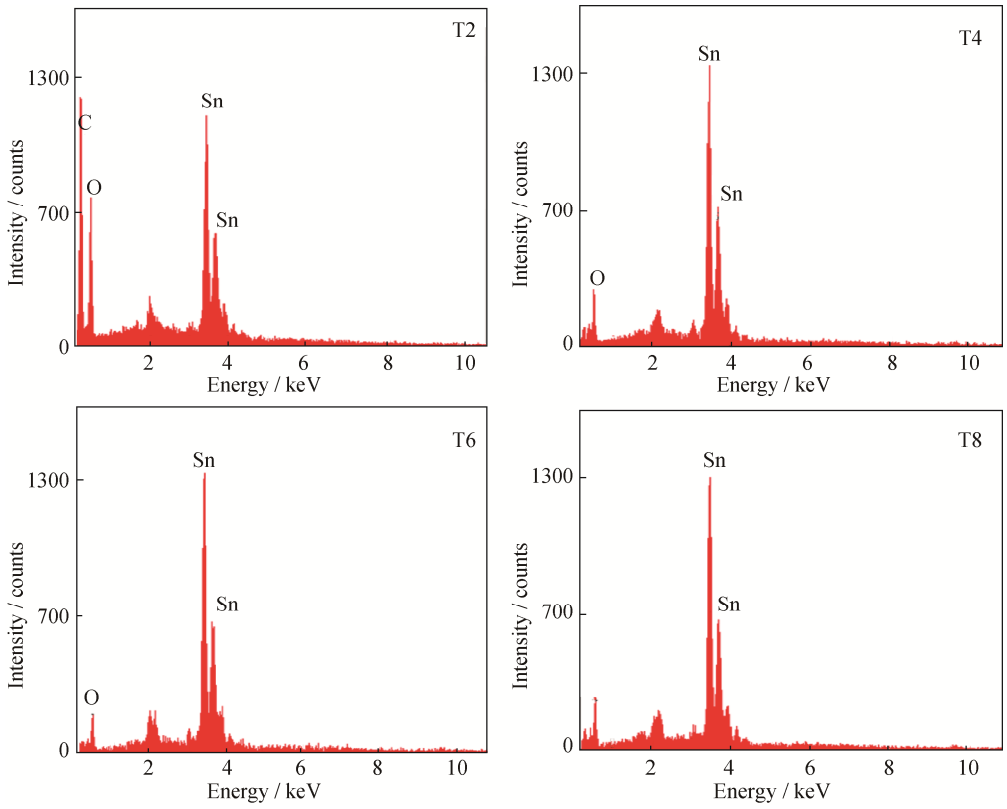

Fig. 5. EDX patterns of Fig. 4.

In the Tauc plot, where $(\alpha hv)^2$ is plotted as a function of hv, the linear portion of the curve is extrapolated to $(\alpha hv)^2$ = 0 and the direct band-gap of the SnO_2 nanoparticles is extracted, as shown in Fig. 6. The band-gap of the T0 sample is 4.412(6) eV. After the annealing process, the band-gaps of samples T2, T4, T6 and T8 were red-shifted to 4.29(1), 3.922(5), 3.856(3), and 3.743(8) eV as a consequence of the agglomeration of the nanoparticles into larger crystallites [35]. With increasing annealing temperature, the band-gap decreases, which is ascribed to a decrease in the carrier concentration and the presence of unoccupied electronic states [36]. In addition, lower band-gaps of 3.580(3) and 3.476(3) eV were observed in samples T0 and T2 because of the creation of impurity levels below the conduction band. In this case, the electrons from the filled valence band are easily excited and enter into a new energy level, simultaneously increasing the number of holes in the valence band. When the annealing temperature exceeds 200°C, the new energy state vanishes, indicating the removal of impurities [37]. This effect is also evidenced by the EDX spectra, which show the disappearance of carbon impurities.

3.5. Photoluminescence spectrophotometry

Fig. 7 shows the PL spectra of the SnO_2 nanoparticles annealed at different temperatures. The O vacancy defects were studied using these spectra. In the luminescence process, O defects act as radiative centers. The O vacancies occur near the surface of nanoparticles, as confirmed by the emission band in the blue-green region. The enhancement in the UV emission intensity is due to a reduction in hydroxyl content. The PL intensity is determined by the structure and size of the nanoparticles. The peak at 365 nm is attributed to the near-band-edge exciton photoluminescence. The increase in intensity of the peak in the UV region with increasing annealing temperature is due to the reduction of the O_2 level. The band-edge emission occurred at 360 nm,

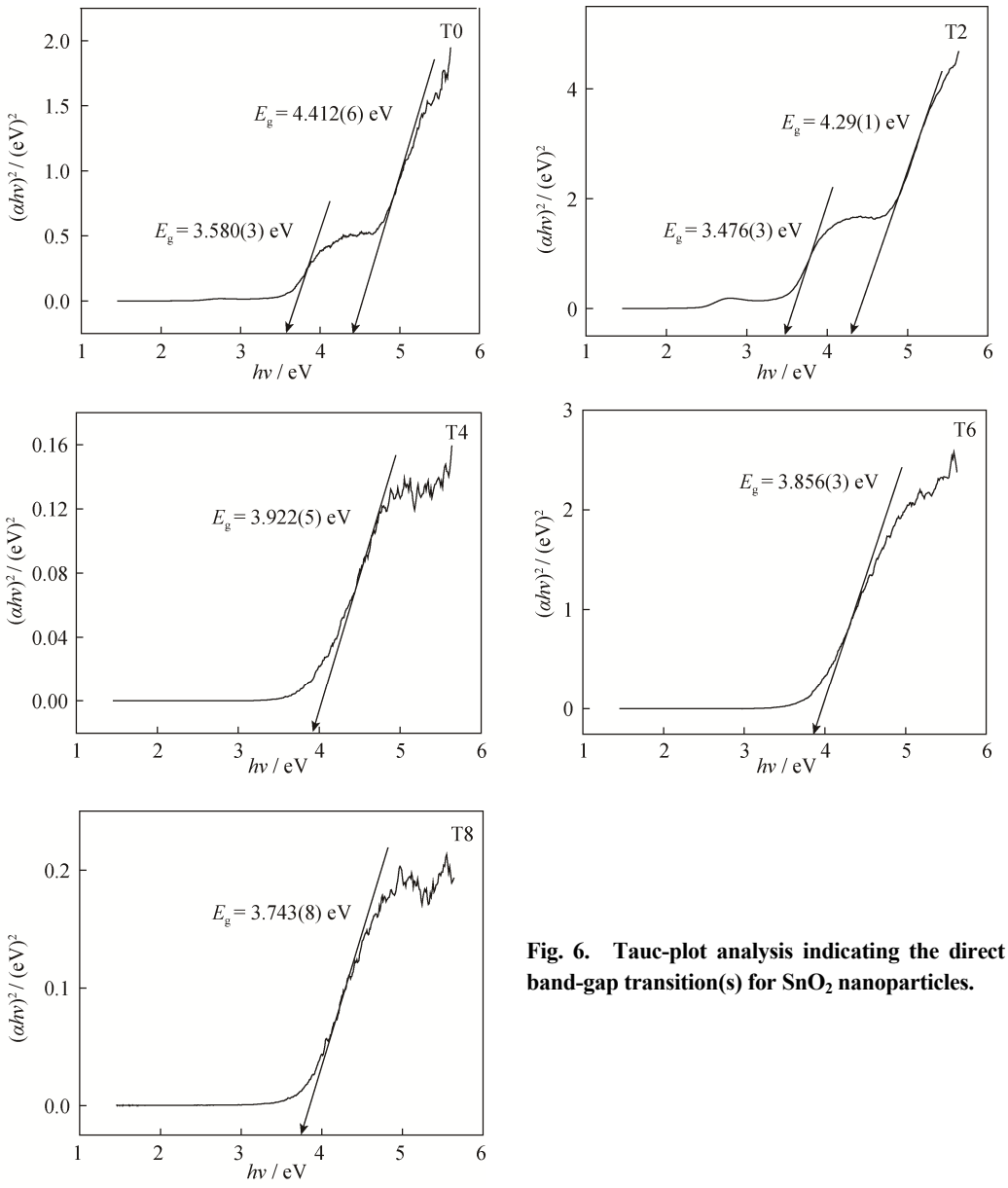

Fig. 6. Tauc-plot analysis indicating the direct band-gap transition(s) for SnO_2 nanoparticles.

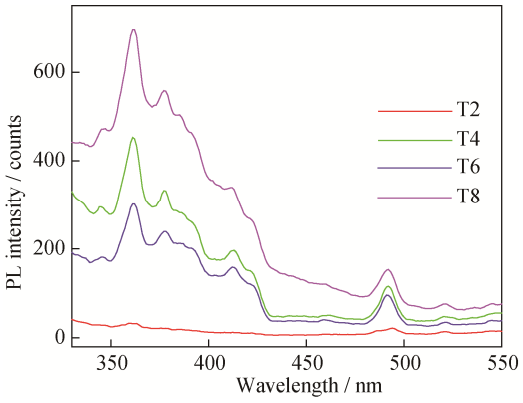

Fig. 7. PL spectra of SnO_2 nanoparticles.

which well matches the band-gap calculated from the UV–Vis spectra. SnO_2 nanoparticles with a highly crystalline structure are known to exhibit intense UV emission [38]. Indeed, the green-synthesized T8 sample exhibits the most intense UV emission among the investigated samples. This intense emission is due to the recombination of holes in the valence band with the electrons in the conduction band, which is the band gap for SnO_2 nanoparticles. The peak at 360 nm is assigned as the recombination of the band-to-acceptor transition [39,40]. The peak at 378 nm is attributed to recombination of donor–acceptor pairs [41].

The relationship between the defect levels within the band gap of SnO_2 nanoparticles and interstitial Sn is con-

firmed by the weak emission peak in the visible region (490 nm) [35]. The increase in the crystalline nature and PL emission intensity, along with the decrease in band gap, indicate that these green-synthesized SnO_2 nanoparticles exhibit desirable properties for catalysis applications.

4. Conclusions

SnO_2 nanoparticles were successfully synthesized using *Camellia sinensis* extract via a green method, without the use of toxic chemicals. The crystallite size of the nanoparticles increased with increasing annealing temperature, and the particles were in the nanometer range, with sizes smaller than 20 nm. Observations of their morphology using HR-SEM revealed that the particles were spherical in shape, with sizes ranging from 5 to 30 nm; this size was confirmed by XRD analysis using the Scherrer equation. TEM images clearly revealed that the particle shape transforms into a hexagonal shape with increasing annealing temperature. The optical band gap energy decreased with increasing annealing temperature, and both UV and visible emission were observed in the PL spectra. Overall, the results presented herein demonstrate that our green-synthesized SnO_2 nanoparticles are promising candidates for future application in catalysis and optoelectronics.

Acknowledgement

One of the authors (Celina Selvakumari) is thankful to the UGC Basic Science Research Fellowship Grant for financial support. We acknowledge the Sophisticated Analytical Instruments Facility, Chennai for SEM, the Sophisticated Test and Instrumentation Centre, Cochin for TEM measurements, and the Department of Physics, Alagappa University for PL measurements.

References

[1] H. Sharghi, S. Ebrahimpourmoghaddam, R. Memarzadeh, and S. Javadpour, Tin oxide nanoparticles (NP-SnO_2): preparation, characterization and their catalytic application in the Knoevenagel condensation, *J. Iran. Chem. Soc.*, 10(2013), No. 1, p. 141.

[2] R.S. Kalubarme, J.Y. Lee, and C.J. Park, Carbon encapsulated tin oxide nanocomposites: An efficient anode for high performance sodium-ion batteries, *ACS Appl. Mater. Interfaces*, 7(2015), No. 31, p. 17226.

[3] M. D'Arienzo, D. Cristofori, R. Scotti, and F. Morazzoni, New insights in the SnO_2 sensing mechanism based on the properties of shape controlled tin oxide nanoparticles, *Chem. Mater.*, 25(2013), No. 18, p. 3675.

[4] H. Chae, D. Song, Y.G. Lee, T. Son, W. Cho, Y.B. Pyun, T.Y. Kim, J.H. Lee, F.F. Santiago, J. Bisquert, and Y.S. Kang, Chemical effects of tin oxide nanoparticles in polymer electrolytes-based dye-sensitized solar cells, *J. Phys. Chem. C*, 118(2014), No. 30, p. 16510.

[5] S. Sudhaparimala, A. Gnanamani, and A.B. Mandal, Green synthesis of tin based nanomedicine: Assessment of microstructure and surface property, *Am. J. Nanosci. Nanotechnol.*, 2(2014), No. 4, p. 75.

[6] H.S. Desarkar, P. Kumbhakar, and A.K. Mitra, Optical properties of tin oxide nanoparticles prepared by laser ablation in water: Influence of laser ablation time duration and laser fluence, *Mater. Charact*., 73(2012), p. 158.

[7] Q.Q. Zhao, L.S. Ma, Q. Zhang, C.G. Wang, and X.J. Xu, SnO_2-based nanomaterials: Synthesis and application in lithium-ion batteries and supercapacitors, *J. Nanomater.*, 2015(2015), art. No. 850147.

[8] S. Sagadevan, Preparation, structural and electrical properties of tin oxide nanoparticles, *J. Nanomater. Mol. Nanotechnol.*, 4(2015), No. 1, p. 889.

[9] S. Nilavazhagani, S. Muthukumaran, and M. Ashokkumar, Microstructural and band gap exploration on Ni-doped SnO_2 nanoparticles co-doped with Cu, *J. Mater. Sci. Mater. Electron.*, 26(2015), No. 6, p. 3989.

[10] V. Juttukonda, R.L. Paddock, J.E. Raymond, D. Denomme, A.E. Richardson, L.E. Slusher, and B.D. Fahlman, Facile synthesis of tin oxide nanoparticles stabilized by dendritic polymers, *J. Am. Chem. Soc.*, 128(2006), No. 2, p. 420.

[11] S.C. Wang and M.O. Shaikh, A room temperature H_2 sensor fabricated using high performance Pt-loaded SnO_2 nanoparticles, *Sensors*, 15(2015), No. 6, p. 14286.

[12] A. Bhattacharjee and Md. Ahmaruzzaman, Photocatalytic-degradation and reduction of organic compounds using SnO_2 quantum dots (via a green route) under direct sunlight, *RSC Adv.*, 5(2015), No. 81, p. 66122.

[13] A.R. Kamali and D.J. Fray, Tin-based materials as advanced anode materials for lithium ion batteries: A review, *Rev. Adv. Mater. Sci.*, 27(2011), No. 1, p. 14.

[14] Y.H. Zhou, J.W. Shim, C. Fuentes-Hernandez, A. Sharma, K.A. Knauer, A.J. Giordano, S.R. Marder, and B. Kippelen, Direct correlation between work function of indium-tin-oxide electrodes and solar cell performance influenced by ultraviolet irradiation and air exposure, *Phys. Chem. Chem. Phys.*, 14(2012), No. 34, p. 12014.

[15] S. Gnanam and V. Rajendran, Synthesis of tin oxide nanoparticles by sol–gel process: effect of solvents on the optical properties, *J. Sol-Gel Sci. Technol*., 53(2010), No. 3, p. 555.

[16] K.C. Song and Y. Kang, Preparation of high surface area tin oxide powders by a homogeneous precipitation method, *Mater. Lett.*, 42(2000), No. 5, p. 283.

[17] G.E. Patil, D.D. Kajale, V.B. Gaikwad, and G.H. Jain, Preparation and characterization of SnO_2 nanoparticles by hydrothermal route, *Int. Nano Lett.*, 2(2012), p. 17.

[18] Z.L. He and J.Q. Zhou, Synthesis, characterization and activity of tin oxide nanoparticles: Influence of solvothermal time on photocatalytic degradation of rhodamine B, *Mod. Res. Catal.*, 2(2013), p. 13.

[19] A. Diallo, E. Manikandan, V. Rajendran, and M. Maaza, Physical and enhanced photocatalytic properties of green synthesized SnO_2 nanoparticles via *Aspalathus linearis*, *J. Alloys Compd.*, 681(2016), p. 561.

[20] E. Haritha, S.M. Roopan, G. Madhavi, G. Elango, N.A. Al-Dhabi, and M.V. Arasu, Green chemical approach towards the synthesis of SnO_2 NPs in argument with photocatalytic degradation of diazo dye and its kinetic studies, *J. Photochem. Photobiol. B*, 162(2016), p. 441.

[21] L. Fu, Y. Zheng, Q. Ren, A. Wang, and B. Deng, Green biosynthesis of SnO_2 nanoparticles by plectranthus amboinicus leaf extract their photocatalytic activity toward rhodamine B degradation, *J. Ovonic Res.*, 11(2015), No. 1, p. 21.

[22] A. Bhattacharjee and M. Ahmaruzzaman, Facile synthesis of SnO_2 quantum dots and its photocatalytic activity in the degradation of eosin Y dye: A green approach, *Mater. Lett.*, 139(2015), p. 418.

[23] Y.H. Zheng, L. Fu, F.G. Han, A.W. Wang, W. Cai, J.P. Yu, J. Yang, and F. Peng, Green biosynthesis and characterization of zinc oxide nanoparticles using *Corymbia citriodora* leaf extract and their photocatalytic activity, *Green Chem. Lett. Rev.*, 8(2015), No. 2, p. 56.

[24] N. Srivastava and M. Mukhopadhyay, Biosynthesis of SnO_2 nanoparticles using bacterium *Erwinia herbicola* and their photocatalytic activity for degradation of dyes, *Ind. Eng. Chem. Res.*, 53(2014), No. 36, p. 13971.

[25] Y.H. Zheng, A.W. Wang, W. Cai, Z. Wan, F. Peng, Z. Liu, and L. Fu, Hydrothermal preparation of reduced graphene oxide–silver nanocomposite using *Plectranthus amboinicus* leaf extract and its electrochemical performance, *Enzyme Microb. Technol.*, 95(2016), p. 112.

[26] S. Begum, Th.B. Devi, and M. Ahmaruzzaman, L-lysine monohydrate mediated facile and environment friendly synthesis of SnO_2 nanoparticles and their prospective applications as a catalyst for the reduction and photodegradation of aromatic compounds, *J. Environ. Chem. Eng.*, 4(2016), No. 3, p. 2976.

[27] G. Elango and S.M. Roopan, Efficacy of SnO_2 nanoparticles toward photocatalytic degradation of methylene blue dye, *J. Photochem. Photobiol. B*, 155(2016), p. 34.

[28] L. Fu and Z.X. Fu, *Plectranthus amboinicus* leaf extract–assisted biosynthesis of ZnO nanoparticles and their photocatalytic activity, *Ceram. Int.*, 41(2015), No. 2, p. 2492.

[29] A. Dasgupta and K. Klein, *Antioxidants in Food, Vitamins and Supplements: Prevention and Treatment of Disease*, Elsevier, p. 239.

[30] H. Nagabhushana, R.B. Basavaraj, B.D. Prasad, S.C. Sharma, H.B. Premkumar, Udayabhanu, and G.R. Vijayakumar, Facile EGCG assisted green synthesis of raspberry shaped CdO nanoparticles, *J. Alloys Compd.*, 669(2016), p. 232.

[31] P. Sutradhar and M. Saha, Synthesis of zinc oxide nanoparticles using tea leaf extract and its application for solar cell, *Bull. Mater. Sci.*, 38(2015), No. 3, p. 653.

[32] P. Sutradhar, M. Saha, and D. Maiti, Microwave synthesis of copper oxide nanoparticles using tea leaf and coffee powder extracts and its antibacterial activity, *J. Nanostruct. Chem.*, 4(2014), p. 86.

[33] J. Wang, H.Q. Fan, H.W. Yu, and X. Wang, Synthesis and optical properties of SnO_2 structures with different morphologies via hydrothermal method, *J. Mater. Eng. Perform.*, 24(2015), No. 9, p. 3426.

[34] J. Nemeth, I. Dekany, K. Suvegh, T. Marek, Z. Klencsar, A. Vertes, and J.H. Fendler, Preparation and structural properties of tin oxide–montmorillonite nanocomposites, *Langmuir*, 19(2003), No. 9, p. 3762.

[35] M.J. Han, K. Jiang, J.Z. Zhang, W.L. Yu, Y.W. Li, Z.G. Hu, and J.H. Chu, Structural, electronic band transition and optoelectronic properties of delafossite $CuGa_{1-x}Cr_xO_2 (0 \le x \le 1)$ solid solution films grown by sol–gel method, *J. Mater. Chem.*, 22(2012), No. 35, p. 18463.

[36] Ayeshamariam, S. Ramalingam, M. Bououdina, and M. Jayachandran, Preparation and characterizations of SnO_2 nanopowder and spectroscopic (FT-IR, FT-Raman, UV-Visible and NMR) analysis using HF and DFT calculations, *Spectrochim. Acta Part A*, 118(2014), p. 1135.

[37] S.A. Ansari and M.H. Cho, Highly visible light responsive, narrow band gap TiO_2 nanoparticles modified by elemental red phosphorus for photocatalysis and photoelectrochemical applications, *Sci. Rep.*, 6(2016), art. No. 25405.

[38] A. Kar, S. Kundu, and A. Patra, Surface defect-related luminescence properties of SnO_2 nanorods and nanoparticles, *J. Phys. Chem. C*, 115(2011), No. 1, p. 118.

[39] B. Liu, C.W. Cheng, R. Chen, Z.X. Shen, H.J. Fan, and H.D. Sun, Fine structure of ultraviolet photoluminescence of tin oxide nanowires, *J. Phys. Chem. C*, 114(2010), No. 8, p. 3407.

[40] W. Chen, D. Ghosh, and S.W. Chen, Large-scale electrochemical synthesis of SnO_2 nanoparticles, *J. Mater. Sci.*, 43(2008), No. 15, p. 5291.

[41] E.R. Viana, J.C. González, G.M. Ribeiro, and A.G. de Oliveira, Photoluminescence and high-temperature persistent photoconductivity experiments in SnO_2 nanobelts, *J. Phys. Chem. C*, 117(2013), No. 15, p. 7844.